

Angular momentum transport and its scaling in co-rotating suspension Taylor-Couette flow

Manojit Ghosh^{1,2,*} and Meheboob Alam^{1,**}

¹Engineering Mechanics Unit, Jawaharlal Nehru Centre for Advanced Scientific Research, Jakkur P.O., Bengaluru 560064, India

²Center of Applied Space Technology and Microgravity (ZARM), University of Bremen, 28359 Bremen, Germany

Abstract.

Torque measurements are carried out to elucidate the global response of a neutrally buoyant, non-colloidal suspension in the co-rotation regime (i.e., the rotation ratio $\Omega = \omega_o/\omega_i > 0$, with ω_o and ω_i being the angular speeds of the inner and outer cylinders, respectively) of Taylor-Couette flow (TCF) up to a shear Reynolds number of $Re_s \leq 1000$ and particle volume fraction of $\phi \leq 0.2$. The dimensional torque increases with increasing particle loading for all $\Omega \leq 0.65$, however, the maximum of dimensionless angular momentum (pseudo Nusselt number) occurs at intermediate values of $\Omega \in (0.3, 0.5)$, depending on the values of Re_s and ϕ . The pseudo-Nusselt number in the co-rotation regime is found to follow the master scaling relation proposed by Alam and Ghosh [Phil. Trans. R. Soc. A 381, 20220226 (2023)] in the counter-rotation regime ($\Omega < 0$). The effect of co-rotation on torque scaling is also discussed.

1 Introduction

The transport of mass, momentum, and energy in fluid flows is a fundamental phenomenon encountered in a wide array of practical applications. The quantification of such transports in complex and arbitrary geometries poses a considerable challenge to our understanding of fluid dynamics, and the simplified models are often employed, offering deeper insights into the underlying mechanisms of transport processes. The fluid flow between two independently rotating concentric cylinders, known as Taylor-Couette flow (TCF), is one such canonical fluid-dynamics problem that has served as a paradigm for studying instabilities and pattern transitions, leading to chaos and turbulence, over the past century, illuminating angular momentum transport across the gap between two cylinders [1–5].

Recent studies [6–8] reveal that the addition of neutrally buoyant, non-colloidal rigid particles to Newtonian fluids can significantly alter the flow transitions in TCF. Specifically, if the particle loading ϕ exceeds a critical value $\phi^{cr} \sim 0.05$, TCF exhibits ‘particle-induced’ primary states, namely, the ribbon (RIB) and/or spiral vortex flow (SVF) and co-existing/mixed states, such as Taylor vortex flow (TVF) + wavy Taylor vortex (WTV) and TVF+SVF. While these flow states are known to affect the global angular momentum transport, given by the torque measured at the inner cylinder [7, 9, 10], the work of Alam and Ghosh [11] came out with a master scaling relation for the dimensionless torque in the counter-rotation regime of TCF ($\Omega \leq 0$). The present study aims to shed light on the angular momentum transport and its scaling in the co-

rotating regime ($\Omega > 0$) of suspension TCF by extending our work [11] in the counter-rotation regime.

2 Experimental methodology

The experimental set-up and methodology are identical to our recent work [8]. A Taylor-Couette (TC) cell, mounted on a Twin-Drive MCR-702 rheometer (Anton Paar GmbH, Austria), is used to perform all the experiments. The inner and outer cylinders of the TC cell are driven via two independently rotating motors by specifying the rotation ratio $\Omega = \omega_o/\omega_i = f_o/f_i$ in the ‘co-rotation’ regime ($\Omega > 0$). The geometrical parameters of the TC cell are the radius ratio $\eta = r_i/r_o \approx 0.89$ and the aspect ratio $\Gamma = h/\delta = h/(r_o - r_i) \approx 8.46$, with $(r_i, r_o, h) = (16.0, 17.95, 16.5)$ mm. A density-matched suspension of rigid PMMA microspheres (mean diameter $d \approx 50 \mu\text{m}$) in a Newtonian solvent (ternary mixture of water, glycerine, and ammonium thiocyanate) is used as the working fluid. For other details on experiments, we refer readers to our previous studies on suspension TCF [8, 11, 12].

At specified (Ω, ϕ) , all experiments consist of a ramp-up protocol, called ‘up-sweep’ run, where the rotation frequency is increased slowly in steps from $f = f_{min} \sim 0$ to $f = f_{max} = \max\{f_i, f_o\} = 50$ Hz by staying 10 s at each step. The number of steps and the step size for up-sweep runs are determined from the dimensionless ramping rate which is set to $|dRe(\phi)/d\tau| = 0.05/\mu_r(\phi)$, where $Re(\phi) = \max\{Re_i(\phi), Re_o(\phi)\}$, with $Re_i(\phi) = \rho\omega_i r_i \delta/\mu(\phi)$ and $Re_o(\phi) = \rho\omega_o r_o \delta/\mu(\phi)$ representing the inner and outer Reynolds numbers, respectively, and $\tau = t/\tau_{vis}$, with $\tau_{vis} = \rho\delta^2/\mu(\phi)$ being the viscous diffusion time;

*e-mail: manojitmath@gmail.com

**e-mail: meheboob@jncast.ac.in

$\mu(\phi) = \mu(0)(1 - \phi/\phi_m)^{-2}$ is the shear viscosity of the suspension, $\mu(0) \approx 7.90$ mPa s is the solvent viscosity, both measured by a rheometer and $\mu_r(\phi) = \mu(\phi)/\mu(0) \geq 1$ is the relative viscosity of the suspension. All experiments are conducted in an air-conditioned room at $T = 22 \pm 0.5^\circ\text{C}$.

A small amount of anisotropic mica flakes is added to the suspension for flow visualizations. Three 41 W LED panels are used to illuminate the TC cell. A Nikon (D750 DSLR) camera is used for continuous imaging of surface flow patterns at a frame rate of 60 s^{-1} , while a Phantom v9 (DANTEC DYNAMICS) camera is used for high-speed imaging at regular intervals at a frame rate of 200 s^{-1} . The torque exerted by the fluid on the inner cylinder is measured by the upper motor of the rheometer and stored by the RheoCompass software on a desktop computer. We use this raw dimensional torque data to perform further analyses as discussed below.

3 Results and discussion

3.1 Dimensionless torque and the maximal transport of angular momentum

Figures 1(a) and 1(b) show the variation of measured dimensional torque \mathcal{T} (in mN-m) with the ‘fluid’ Taylor number $\text{Ta}(0) = \mu_r^2 \text{Ta}(\phi)$ (defined in terms of the viscosity of the solvent $\mu(0)$), or, the fluid shear Reynolds number $\text{Re}_s(0) = \mu_r \text{Re}_s(\phi)$ for up-sweep runs at $\Omega = 0.05$ and $\Omega = 0.65$, respectively; here, $\text{Ta}(\phi) = \sigma^2 \text{Re}_s(\phi)^2$ is the Taylor number, with $\sigma = (1 + \eta)^4 / 16\eta^2$ being the ‘geometrical’ Prandtl number, and

$$\text{Re}_s(\Omega, \phi) = \frac{2}{1 + \eta} |1 - \Omega| \text{Re}_i(\phi) = \frac{2\eta}{1 + \eta} \frac{|1 - \Omega|}{\Omega} \text{Re}_o(\phi) \quad (1)$$

is the shear Reynolds number [13, 14]. Note that while $\Omega = 0.05 \sim 0$ refers to a nearly stationary outer cylinder, $\Omega = 0.65$ is closer to the Rayleigh line $\Omega = \eta^2 \approx 0.8$ [16] beyond which TCF remains stable. In each panel of Fig. 1(a,b), triangles, circles, stars, and diamonds mark the primary, secondary, tertiary, and quaternary bifurcations, respectively. The bifurcations among various flow states were recently explored by Ghosh and Alam [8] who reported that the primary bifurcating state is TVF for $\phi < 0.1$, while RIB and/or SVF emerge as the primary state at $\phi \geq 0.1$. Moreover, at $\Omega = 0.05$, the primary states (TVF/RIB/SVF) go through transitions with increasing $\text{Ta}(0)$, leading to a higher-order state WTV. On the contrary, the WTV is found to be absent at $\Omega = 0.65$ within the explored range of $\text{Ta}(0)$.

From Fig. 1(a,b), it is evident that at a specified rotation ratio, the dimensional torque increases with increasing particle loading ϕ . Since the effective viscosity of suspension also increases with ϕ , it is instructive to consider a dimensionless measure of the torque, defined as $G = \mathcal{T} \rho / 2\pi h \mu(\phi)^2$. A more useful representation of the dimensionless torque is the ‘pseudo’ or ‘omega’ Nusselt number [11, 13, 14], defined via

$$\text{Nu}_\omega \stackrel{\text{def}}{=} \frac{J^\omega}{J_{\text{lam}}^\omega} = \frac{G}{G_{\text{lam}}}, \quad (2)$$

where $J^\omega = \mu(\phi)^2 G / \rho^2$ is the angular velocity flux from inner to the outer cylinder and $J_{\text{lam}}^\omega = \mu(\phi)^2 G_{\text{lam}} / \rho^2$ is its laminar counterpart, with $G_{\text{lam}} = \eta \sqrt{\text{Ta}(0)} / \mu_r \sigma (1 - \eta)^2$ being the dimensionless laminar torque for a TC cell having an infinite aspect ratio [13, 14]. Thus, Nu_ω provides an estimate of the dimensionless angular momentum transfer by comparing the transfer efficiency of the convective mechanism to purely molecular transport in radial direction.

The effects of particle loading and co-rotation on Nu_ω are displayed in Fig. 2(a,b). While Fig. 2(a) illustrates the variation of Nu_ω with Ω for different $\text{Ta}(0)$ for the particle-free ($\phi = 0$) Newtonian fluid, Fig. 2(b) shows the same for a suspension with $\phi = 0.15$. By comparing Figs. 2(a) and 2(b), we find that for fixed $\text{Ta}(0)$ the normalized torque Nu_ω decreases with increasing particle loading at all Ω .

From Fig. 2(a) ($\phi = 0$), we find that Nu_ω gradually increases with Ω when $\text{Ta}(0)$ is relatively small, i.e., $\text{Ta}(0) \leq 2.33 \times 10^4$; however, at moderate values of $\text{Ta}(0)$, i.e., for $2.33 \times 10^4 < \text{Ta}(0) \leq 3.72 \times 10^5$, Nu_ω increases till $\Omega = 0.5$ before decreasing at $\Omega = 0.65$. This indicates that beyond the primary bifurcation, the maximum transport of dimensionless angular momentum takes place around $\Omega \approx 0.5$. The latter can also be identified from Fig. 2(c) where the location of torque maximum is shown over a range of $\text{Ta}(0)$. From Fig. 2(a,c), we find that for $\text{Ta}(0) > 3.72 \times 10^5$, the torque maximum occurs at $\Omega = 0.3$ and then shifts towards smaller Ω as $\text{Ta}(0)$ increases further. Similar non-monotonic dependence of Nu_ω on the rotation ratio Ω as well as the shifting of $\text{Nu}_\omega^{\text{max}}$ towards smaller Ω was reported by Brauckman *et al.* [15].

In the presence of particles (see Fig. 2b,c at $\phi = 0.15$), we find that Nu_ω increases with Ω at smaller values of $\text{Ta}(0)$, indicating the location of torque maximum at $\Omega = 0.65$. Interestingly, at moderate values of $\text{Ta}(0)$, i.e., for $5.74 \times 10^4 < \text{Ta}(0) \leq 1.51 \times 10^5$, the location of torque maximum is found to switch between $\Omega = 0.5$ and $\Omega = 0.65$, illustrating the non-trivial effect of particles on the angular momentum transport process. At further higher values of $\text{Ta}(0)$, the torque maximum occurs at $\Omega = 0.5$ before moving towards smaller Ω with further increasing $\text{Ta}(0)$ (Fig. 2c). It should be noted that the accessible range of $\text{Ta}(0)$ reduces with increasing Ω in present experiments; therefore, at higher $\text{Ta}(0)$, the torque maximum spans a narrower range of Ω , and hence no firm conclusion can be drawn regarding the location of $\text{Nu}_\omega^{\text{max}}$ in terms of (Ω, ϕ) .

3.2 Master scaling relation for torque

We follow the procedure described in Ref. [11] to derive torque scaling within the explored range of $\text{Ta}(0)$ in the co-rotation regime of present experiments. To this end, we first calculate the ‘bare’ pseudo Nusselt number, defined by

$$\text{Nu}_{\omega 0} \stackrel{\text{def}}{=} \frac{G(\phi = 0)}{G_{\text{lam}}(\phi = 0)} = \frac{G_0}{G_{\text{lam}0}} = \mu_r \text{Nu}_\omega, \quad (3)$$

where $G_0 = \mu_r(\phi)^2 G(\phi)$ is the dimensionless torque for a particle-free Newtonian fluid and $G_{\text{lam}0} = \mu_r(\phi) G_{\text{lam}}(\phi)$ is its value in the laminar (CCF) state. Next, we calculate two compensated Nusselt numbers [11]: $\text{Nu}_{01} = \text{Nu}_{\omega 0} \text{Ta}(0)^k$

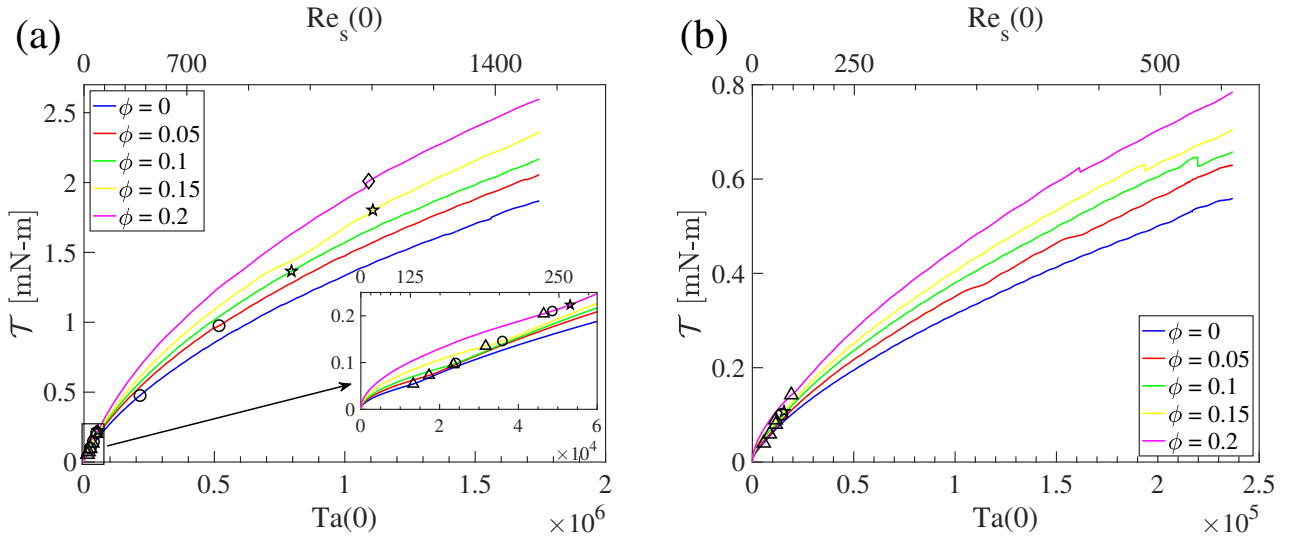


Figure 1: Variation of dimensional torque \mathcal{T} (in mN-m) with $Ta(0) = \mu_r^2 Ta(\phi)$, or, $Re_s(0) = \mu_r Re_s(\phi)$ at (a) $\Omega = 0.05$ and (b) $\Omega = 0.65$ for up-sweep runs. The open triangles, circles, stars, and diamonds, respectively, represent the critical values of $Ta(0)$ where primary, secondary, tertiary, and quaternary transitions take place.

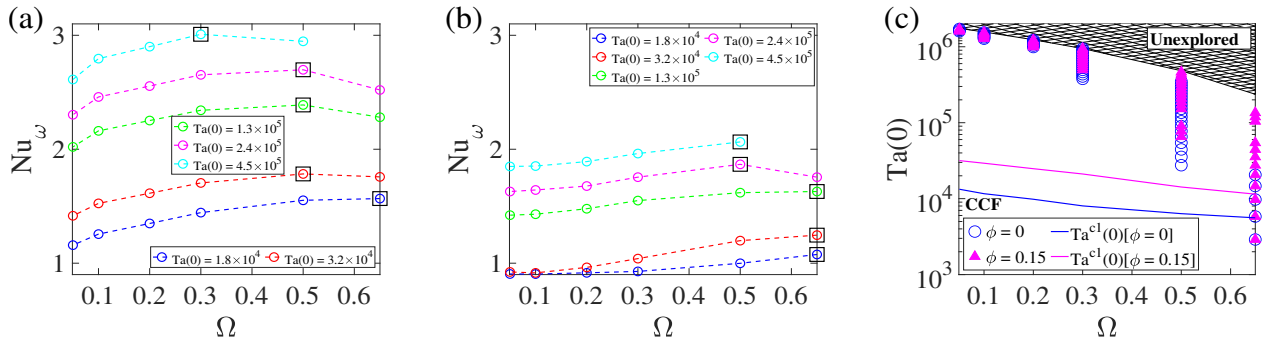


Figure 2: (a,b) Variations of normalized torque Nu_ω with Ω at specified $Ta(0)$ for (a) $\phi = 0$ and (b) $\phi = 0.15$ during up-sweep runs. The empty black squares in (a,b) mark the location of torque maximum or Nu_ω^{max} . (c) Location of Nu_ω^{max} at given $Ta(0)$. The blue and magenta lines in (c) mark the CCF \rightarrow TVF boundary at $\phi = 0$ and CCF \rightarrow RIB boundary at $\phi = 0.15$, respectively.

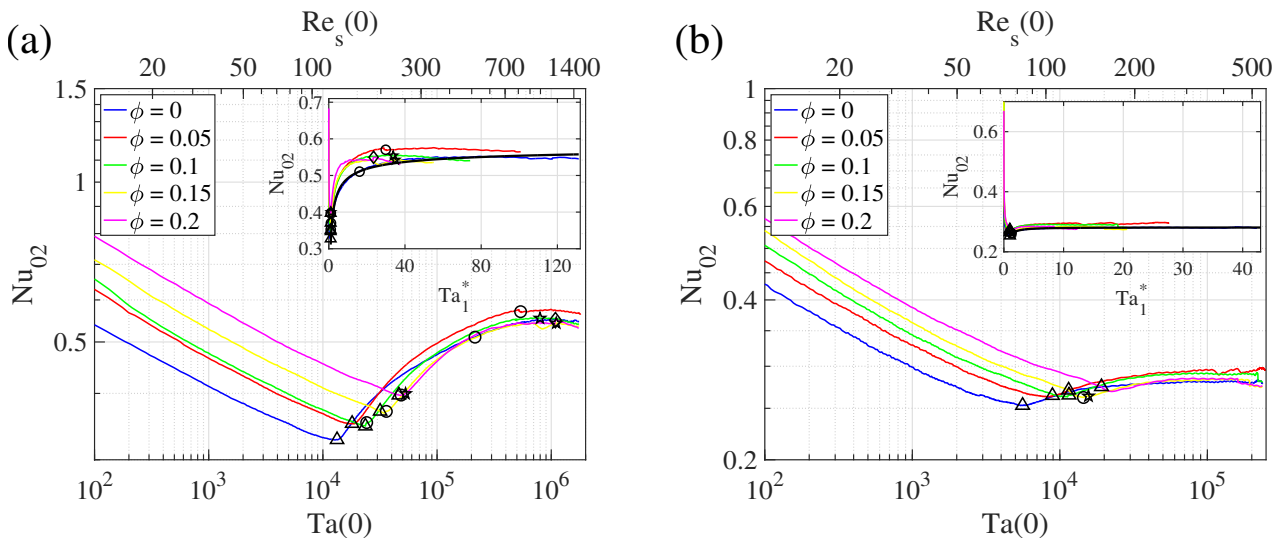


Figure 3: Main panels show the variations of $Nu_{02} = Nu_{01} \mu_r^n = Nu_\omega Ta(0)^k \mu_r^n$ with $Ta(0)$ at (a) $\Omega = 0.05$ and (b) $\Omega = 0.65$. Insets show the same with Ta_1^* . The black curve in each inset represents the least-square fit at $Ta_1^* \geq 1$.

Table 1: Exponents (k, n) and pre-factors ($\alpha_0, \alpha_1, \alpha_2$) at different Ω for the scaling relations (6) and (9).

Ω	k	n	α_0	α_1	α_2
0.05	0.121	0.425	0.587	-0.274	-0.468
0.5	0.157	0.378	0.441	-0.145	-0.275
0.65	0.178	0.417	0.281	-0.032	-1.2451

and $Nu_{02} = Nu_{01}\mu_r^n = Nu_{\omega 0}Ta(0)^k\mu_r^n$. The variations of Nu_{02} at $\Omega = 0.05$ and $\Omega = 0.65$ are shown in Figs. 3(a) and 3(b), respectively. From the main panel in Fig. 3(a), we find that at $\Omega = 0.05$, beyond the TVF \rightarrow WTV transition, the compensated torque data at different particle loadings collapse approximately onto a single curve for a suitable choice of $(k, n) = (0.121, 0.425)$. On the other hand, the main panel of Fig. 3(b) illustrates that at $\Omega = 0.65$, the compensated torque data corresponding to different ϕ collapse onto a single curve beyond CCF/SVF \rightarrow TVF, or, CCF \rightarrow SVF transitions for $(k, n) = (0.178, 0.417)$. Finally, we find that all the data in the main panels of Figs. 3(a) and 3(b) can be collapsed onto a master curve

$$Nu_{02} = \alpha_0 + \alpha_1 Ta_1^{*\alpha_2}, \quad \text{with } Ta_1^* \geq 1, \quad (4)$$

beyond the primary bifurcation (see the insets of Figs. 3a and 3b) with the introduction of a ‘reduced’ Taylor number, defined by

$$Ta_1^* \stackrel{def}{=} \frac{Ta(\phi)}{Ta^{c1}(\phi)}, \quad (5)$$

here, $Ta^{c1}(\phi)$ is the critical Taylor number for the onset of primary bifurcation (CCF \rightarrow TVF, or, RIB or SVF). The master scaling relation can then be found by rearranging equation (4) as

$$Nu_{\omega 0} = (\alpha_1 Ta_1^{*\alpha_2} + \alpha_0) Ta(0)^k \mu_r^n, \quad (6)$$

with exponents (k, n) and pre-factors ($\alpha_0, \alpha_1, \alpha_2$) being determined from a least-squares fit to the data at $Ta_1^* \geq 1$. Equation (6) can be rearranged further to yield the master scaling for the pseudo/omega-Nusselt number (Nu_{ω}) in terms of $Ta(\phi)$ or $Re_s(\phi)$ as

$$Nu_{\omega} = (\alpha_1 Ta_1^{*\alpha_2} + \alpha_0) Ta(\phi)^k \mu_r^{(2k+n-1)} \quad (7)$$

$$= (\alpha_1 Ta_1^{*\alpha_2} + \alpha_0) \sigma^{2k} Re_s(\phi)^{2k} \mu_r^{(2k+n-1)} \quad (8)$$

$$\approx (\alpha_1 Ta_1^{*\alpha_2} + \alpha_0) Re_s(\phi)^{2k} \mu_r^{(2k+n-1)}, \quad (9)$$

where the last step follows the approximation $\sigma = (1 + \eta)^4 / 16\eta^2 \approx 1.006$ for $\eta = 0.89$ [11].

It is interesting to note that the functional form of torque scaling (9) remains the same as that proposed by Alam and Ghosh [11] for the counter-rotating cylinders ($\Omega \leq 0$); the differences appear only in the values of exponents and pre-factors that can be confirmed by comparing the Table 1 of the present study with that of Ref. [11]. From Table 1, we find that while (k, α_0, α_1) show a monotonic dependence with Ω , (n, α_2) exhibit a non-monotonic behavior through which the effect of co-rotation mainly enters into the scaling relation. The non-monotonicity of

(n, α_2) can be attributed to the maximum transport of angular momentum at $\Omega = (0.3, 0.5)$ beyond the primary bifurcation, for which n is minimum and α_2 is maximum (see Table 1).

While the present torque data pertains to the transitional, pattern-forming regimes of TCF, further experiments are recommended over a larger range of $Ta(0)$ and an extended set Ω to understand the torque scaling in the turbulent regime [17, 18] of suspension TCF at $\Omega > 0$. In addition, it must be noted that the present torque measurements include contributions from two Ekman vortices (adjacent to two axial end-caps) that are expected to become stronger in the co-rotation regime. The role of inertial particles (with particle Reynolds number being $Re_p = O(1)$) on Ekman vortices and the cross-stream migration of particles [19] on angular momentum transport should be probed in the future.

References

- [1] G.I. Taylor, Phil. Trans. R. Soc. Lond. A **223**, 289-343 (1923).
- [2] D. Coles, J. Fluid Mech. **21**, 385-425 (1965).
- [3] C.D. Andereck, S.S. Liu, H.L. Swinney, J. Fluid Mech. **164**, 155-183 (1986).
- [4] S. Grossmann, D. Lohse, C. Sun, Annu. Rev. Fluid Mech. **48**, 53-80 (2016).
- [5] R.M. Lueptow, R. Hollerbach, E. Serre, Phil. Trans. R. Soc. A **381**, 20220140 (2023).
- [6] M.V. Majji, S. Banerjee, J.F. Morris, J. Fluid Mech. **835**, 936-969 (2018).
- [7] P. Ramesh, S. Bharadwaj, M. Alam, J. Fluid Mech. **870**, 901-940 (2019).
- [8] M. Ghosh, M. Alam, J. Fluid Mech. **995**, R4 (2024).
- [9] A. Dash, A. Anantharaman, C. Poelma, J. Fluid Mech. **903**, A20 (2020).
- [10] M. Moazzen, T. Lacassagne, V. Thomy, S.A. Bahrani, J. Fluid Mech. **937**, A2 (2022).
- [11] M. Alam, M. Ghosh, Phil. Trans. R. Soc. A **381**, 20220226 (2023).
- [12] S. P. Singh, M. Ghosh, M. Alam, J. Fluid Mech. **944**, A18 (2022).
- [13] B. Dubrulle, O. Dauchot, F. Daviaud, P. Y. Longaretti, D. Richard, J. P. Zahn, Phys. Fluids **17**, 095103 (2005).
- [14] B. Eckhardt, S. Grossmann, D. Lohse, J. Fluid Mech. **581**, 221-250 (2007).
- [15] H.J. Brauckman, M. Salewski, B. Eckhardt, J. Fluid Mech. **790**, 419-452 (2016).
- [16] L. Rayleigh, Proc. R. Soc. Lond. A **93**, 148-154 (1917).
- [17] M. Avila, Phys. Rev. Lett. **108**, 124501 (2012).
- [18] M.S. Paoletti, D.P.M. van Gills, B. Dubrulle, C. Sun, D. Lohse, D.P. Lathrop, A & A **547**, A64 (2012).
- [19] L. Baroudi., M.V. Majji, J.F. Morris, Phys. Rev. Fluids **5**, 114303 (2020).